Wide-Range, Open-Loop, CCT and Illuminance Control of an LED Lamp Using Two-Component Color Blending

Rajib Malik, Kalyan Kumar Ray, and Saswati Mazumdar

***Abstract*—This paper proposes a wide-range control scheme of correlated color temperature (CCT) and illuminance of a light-emitting diode (LED) lamp, using two-component color blending. A simple control algorithm is implemented by using Grassmann's law of color mixing and McCamy's formula of CCT. Light from a white LED source is blended with that from a blue LED or a red LED to get, respectively, a CCT value higher or lower than that of the white CCT. The prototype LED lighting system can independently produce a variable CCT ranging from 2500 to 12500 K and a variable illuminance ranging from 5 to 120 lx. The algorithm is experimentally validated by hardware implementation. An empirical model to estimate the luminous parameters of the individual LED is also implemented. Experimental results show that although the system is an open-loop one, it is quite accurate with respect to set point CCT and illuminance. Despite acceptable performance in respect of these two quantities, a large deviation from the color of an ideal black body radiator is noticeable in a part of the CCT range, and a remedy of the problem has been suggested.**

***Index Terms*—Color measurement, light sources, light-emitting diodes (LEDs), lighting control, pulse width modulation (PWM).**

I. Introduction

HIGH-BRIGHTNESS light-emitting diodes (HB-LEDs) are becoming the prime candidates for general lighting applications. HB-LEDs have the notable advantages of high luminous efficiency and consequently reduced energy consumption, very low ultraviolet emission, high environment friendliness, and longer operating lifetime over conventional incandescent and fluorescent lamps [1]–[3].

The correlated color temperature (CCT) of daylight can vary from 2000 K at sunrise to 5000 K for direct daylight at noon and can exceed 10 000 K under overcast conditions [4]. Along with the CCT, the illuminance of daylight also varies dynamically. So, to create a near-exact visual sensation and energy-efficient lighting, an artificial light source (visually matched LED lamp), with independently tuneable CCT and illuminance, should preferably be introduced in daylight harvesting schemes [4]. Apart from daylight harvesting, color-tuneable light sources may be used for mood lighting, which affects the emotional feeling of humans [5]–[7]. In a recent study, dark adaption, color discrimination, and fog penetration of street lights have been analyzed under different CCT [8]. CCT-tuneable LED light sources have been used in street lighting to get better visual performance [8]. Thus, the demand of independent CCT and illuminance controllable light sources for various applications is rapidly increasing.

In order to explain the significance of the proposed technology, a review of the existing techniques to produce the CCT-tuneable LED lighting system is provided in this section. Currently, LED-based white light is produced either from a blue or a near-ultraviolet-emitting chip coated with a suitable yellow phosphor, or by mixing of light from multiple monochromatic chips, usually, red, green, and blue (RGB) [9]. In some of the previous studies, light from monochromatic RGB LEDs [10]–[13] or red-green-blue-amber (RGBA) LEDs [4] was mixed to get different color combination of white shade. These types of LED systems have some disadvantages like poor color rendering index (CRI), chromaticity shifts [14], [15], and requirement of three or more pulse-width-modulated (PWM) output channels. It is reported that the chromaticity shift for a phosphor-coated LED (PC-LED) system is less than that of the mixed-color RGB LED (MC-LED) system, during similar dimming by both continuous current reduction and PWM method [14]. Also, this type of the LED system uses three (for RGB) [11], [16] or four (for RGBA) [4] independent converters to supply power as described by the authors. To resolve the issue, we are using a single constant voltage power supply to drive multiple LED strings with individually programmable constant amplitude PWM current, which also increases the power density. Chromaticity of the RGB LED also shifts due to LED junction temperature variation [16], [17] and aging [18]. But the use of an MC-LED system allows the user to have dynamic control of color and a life longer than that of a PC-LED system.

CCT-tuneable light sources have also been implemented by blending cool-white (CW) and warm-white (WW) LED sources [19]–[22]. A number of commercial, tuneable LED-lighting products, e.g., Lutron [23], LuxiTune [24] are also available. Lutron from Philips provides three types of color-tuning techniques, namely "dim to warm," "tuneable white," and "full color tuning" [23]. In tuneable white mode, WW (3000 K) and CW

Manuscript received September 25, 2017; revised November 11, 2017; accepted December 11, 2017. Date of publication December 20, 2017; date of current version August 7, 2018. Recommended for publication by Associate Editor D. G. Lamar. *(Corresponding author: Rajib Malik.)*

R. Malik and S. Mazumdar are with the Department of Electrical Engineering, Jadavpur University, Kolkata 700032, India (e-mail: rajib.diara@gmail.com; saswati.mazumdar@gmail.com).

K. K. Ray is with the Department of Instrumentation and Electronics Engineering, Jadavpur University, Kolkata 700032, India (e-mail: kalyancs.ray@gmail.com).

Digital Object Identifier 10.1109/TPEL.2017.2785684

(5000 K) LED are used to provide different color temperatures ranging from 3000 to 5000 K. In this mode, color temperature and intensity of the fixture are not completely independent as specified in the application note. LuxiTune from LED Engin is a tuneable white light engine solution, with two tuning modes: warm dimming and CCT tuning. CCT can be varied in the range 4300–2100 K and 3000–1600 K in CCT-tuning mode and warm dimming mode, respectively [24]. In such systems, the CRI can be greatly improved, but the CCT of the produced light is limited to a range between that of CW and WW LEDs. However, work on wide-range CCT and illuminance tuneable light sources, based on two channel drive, has not been reported.

Precise color control of PC white LED or RGB color mixing LED system is still a challenging job for the lighting industry [11], [17], [25]–[28]. As luminous intensity and color outputs of LED are influenced by LED junction temperature variation, which is caused by self-heating of the LED and ambient temperature variation, it has been suggested that a proper junction temperature compensated control strategy should be implemented to stabilize the luminous intensity as well as the color of LED [17], [29]–[32]. Various researchers proposed different control structures based on LED junction temperature feedback, light flux feedback, color coordinate feedback or a combination of these techniques [11], [12], [21], [27]. Use of external sensors, which is mandatory for flux feedback and color coordinate feedback, increases the complexity and overall cost of the system. Sensor placement and regular calibration of sensors are important issues which may not be acceptable in all applications. In some previous studies, the junction temperature of an LED is estimated as a function of its heatsink temperature [17] or LED operating temperature [33]. However, when multiple LEDs are mounted on a common heatsink, the junction temperature of a particular LED is not only a function of the heatsink temperature but also of the power dissipation of the neighboring LEDs.

In this paper, a wide-range, open-loop, and decoupled control of CCT and illuminance of a composite LED lamp has been presented that employs two-component color blending. Light from a main CW PC-LED source is mixed in required proportion with that from a companion source which is either a blue or a red LED. Both the sources are fed by linear PWMs. Mathematical formulations necessary for selection of the companion source and determination of the duty cycles of the PW modulators for obtaining the desired CCT and work plane illuminances are derived. Using a hardware made of readily available components and a simple software built for the purpose, a proof-of-concept system has been built. The forward drop of an LED fed by a constant current is a linearly decreasing function of its junction temperature. In our case, no attempt was made to estimate the junction temperature. Instead, the chromaticity coordinates of an LED source and its luminous flux contribution have been estimated from its forward drop, when driven under PWM control with a fixed peak current. The system is capable of providing a CCT range of 2500–12500 K and an illuminance range of 5–120 lx. The principle of operation, the mathematical formulations, and the hardware and software features of the system have been described and performance evaluation of the system has been made through laboratory experiments. This kind of the dynamic LED lighting system can be used in diverse applications like street lighting, human-centric lighting, daylight harvesting, mood lighting, etc.

II. Principle of Two-Component Color Blending

A. Overview of the Proposed RBW LED Lighting System

To resolve the issue related to the limited CCT-tuneable facility as described in the earlier section, in this paper a hybrid LED color mixing scheme has been implemented, where light from a main CW PC-LED source is blended with that from a companion red or a blue LED source to get, respectively, a CCT lower or higher than that of the CW LED. For a required CCT, since only two sources are involved, the color shift of the blended light due to drift of the chromaticity of the constituent sources is less pronounced, provided the luminance and chromaticity shift of the sources are estimated at the runtime and the blending ratio is adjusted accordingly.

A block diagram of the proposed LED lighting system with decoupled control of CCT and illuminance is shown in Fig. 1. Blending of light from the main CW LED with that of companion LED is implemented using PWM dimming technique. The combination of the microcontroller unit (MCU), the demultiplexer (DEMUX), and the human interfaces, shown inside the left-hand rectangle will be termed as CCT and illuminance control unit (CICU). The three voltages, ufa_W, ufa_R, and ufa_B given as inputs to three analog-to-digital converters (ADC) in the CICU are the average forward drops of the three LED strings, which, in turn, are obtained by passing the instantaneous rectangular pulse waveforms through adequate low-pass active filters. Further details of the filters are available in Section III. Other salient hardware features of the system are also given in the same section.

B. Mathematical Foundation of the Control Strategy

Two primary light sources S_1 and S_2 of two different colors with Commision Internationale de l'Eclairage (CIE) 1931 chromaticity coordinates of (x_1, y_1) and (x_2, y_2), respectively, are used to illuminate the same surface (the work plane). Y_1 and Y_2 are their respective luminance values, and E_1 and E_2 are the respective illuminance contributions on the work plane. Grassmann's law [34], [35], also known as the law of linear combination of colors, states that the chromaticity coordinates (x_b, y_b) of the blended color is given by the linear weighted sums of the chromaticity coordinates of S_1 and S_2 given as follows:

$$x_b = x_1 a_1 + x_2 a_2, \quad \text{and} \quad y_b = y_1 a_1 + y_2 a_2 \tag{1}$$

where the weighting coefficients a_1 and a_2 are given by

$$a_1 = \frac{\frac{Y_1}{y_1}}{\frac{Y_1}{y_1} + \frac{Y_2}{y_2}} \quad \text{and} \quad a_2 = \frac{\frac{Y_2}{y_2}}{\frac{Y_1}{y_1} + \frac{Y_2}{y_2}}. \tag{2}$$

It may be observed here that by virtue of definitions of a_1 and a_2

$$a_1 + a_2 = 1. \tag{3}$$

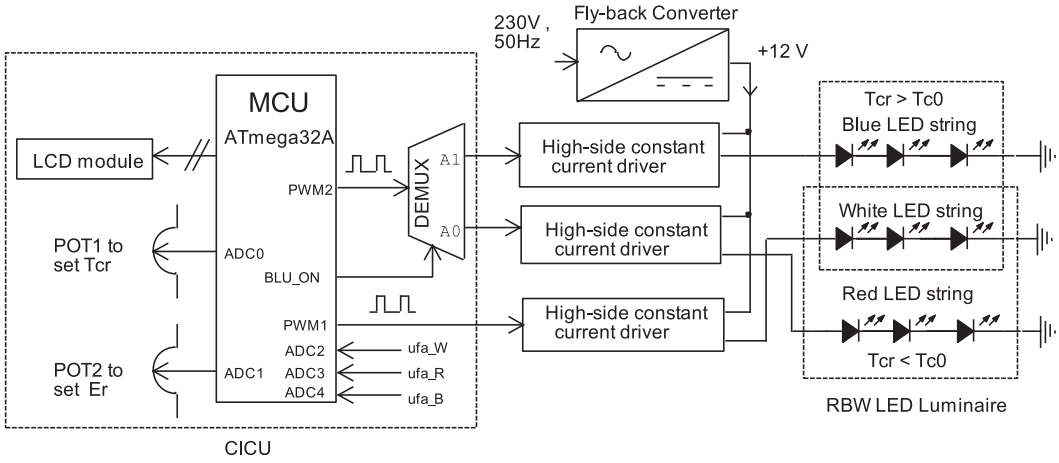

Fig. 1. Block diagram of the proposed CCT and illuminance controllable LED lighting system.

Use of simple analytical geometry shows that, due to (3), the position of (x_b, y_b) coordinate pair in the *xy* plane cannot be arbitrary—it must lie on the straight line joining the coordinate pairs of the constituent sources.

For the purpose of control of the blended color, the two source luminances have to be controlled over a wide range. While analog control of the LED currents is a theoretical option, it cannot be used in this application due to several reasons [14], [36]. The first is that the linearity of the luminance versus current graph is rather poor [36]. Second, the chromaticity changes with change of current [36]. Another important reason is that the generation of an analog current command from a microcontroller requires additional hardware like a digital-to-analog converter (DAC) or a PWM-to-analog converter.

In the present study, the two source luminances are controlled by two linear PWM dimmers described in Section III. If D_1 and D_2 are their respective duty cycles, the values of Y_1 and Y_2 will be given by

$$Y_1 = Y_{M1} D_1 \tag{4}$$

and

$$Y_2 = Y_{M2} D_2 \tag{5}$$

where Y_{M1} and Y_{M2} are the maximum values of Y_1 and Y_2 corresponding to the maximum values of D_1 and D_2, namely, unity. Equations (1)–(5) clearly indicate that by changing the values of D_1 and D_2, the chromaticity coordinates of the blended color (indeed, the color) can be changed.

In many situations, where the distance between the sources and the illuminated surface is fixed, the transmittance of the medium is fixed, reflectances of nearby objects are fixed, and there is no stray light, the following equations in terms of the illuminances E1, E2 can be written:

$$E_1 = k_{\mathrm{YE}} Y_1 \tag{6}$$

$$E_2 = k_{\mathrm{YE}} Y_2 \tag{7}$$

where k_{YE} is a constant.

In view of the linearity of the PWM process, the average or apparent illuminances E_1 and E_2 are related to their respective maximum values E_{M1} and E_{M2} as follows:

$$E_1 = E_{M1} D_1 \tag{8}$$

$$E_2 = E_{M2} D_2. \tag{9}$$

Equation (2) is thus modified as

$$a_1 = \frac{\frac{E_{M1}\ D_1}{y_1}}{\frac{E_{M1}\ D_1}{y_1} + \frac{E_{M2}\ D_2}{y_2}} \text{ and } a_2 = \frac{\frac{E_{M2}\ D_2}{y_2}}{\frac{E_{M1}\ D_1}{y_1} + \frac{E_{M2}\ D_2}{y_2}}. \tag{10}$$

If we define the a_2/a_1 ratio as r_a

$$r_a = \frac{a_2}{a_1} \tag{11}$$

its value, in view of (10), will be given as $r_a = \frac{E_{M2}}{E_{M1}} \frac{D_2}{D_1} \frac{y_1}{y_2}$, or, equivalently,

$$\frac{D_2}{D_1} = r_a \frac{E_{M1}}{E_{M2}} \frac{y_2}{y_1}. \tag{12}$$

The following additional definitions are now made:

$$\text{Peak illuminance ratio}, r_E = \frac{E_{M2}}{E_{M1}} \tag{13}$$

$$y\text{−coordinate ratio}, r_y = \frac{y_2}{y_1} \tag{14}$$

$$\text{Blending ratio}, r_D = \frac{D_2}{D_1}. \tag{15}$$

Equations (13)–(15), when substituted in (12), yield the value of blending ratio r_D as

$$r_D = \frac{r_a\ r_y}{r_E}. \tag{16}$$

Equation (3) along with the first of (1) results in a value of $r_a = a_2/a_1$ as

$$r_a = \frac{x_1 - x_b}{x_b - x_2}. \tag{17}$$

Thus, if the chromaticity coordinate x_b of the required blended light is known, the use of (16) will evaluate the required blending ratio r_D.

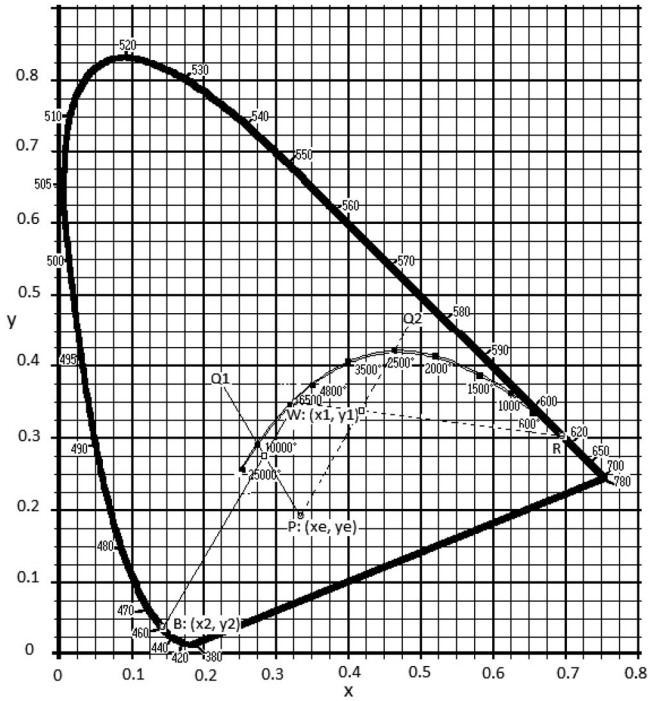

Fig. 2. Blending line, isoCCT line, and Planckian locus shown on the CIE 1931 chromaticity diagram.

The chromaticity coordinates of the two constituent sources and that of the blended light is shown in Fig. 2. For convenience, the line segment joining the two points S_1 and S_2 will be called the blending line. The equation of the blending line can be shown to be given by

$$y = m\,x + (y_2 - m\,x_2) \tag{18}$$

where (x, y) is the coordinate of an arbitrary point on the line and

$$m = \frac{y_2 - y_1}{x_2 - x_1} \tag{19}$$

is the slope of the line. Two blending lines WB (for S_2 = blue) and WR (for S_2 = red), used in this study, are shown in Fig. 2. McCamy's formula [37] for evaluation of the CCT T_c of a source with known xy chromaticity coordinates involves calculating a number n given by

$$n = \frac{x - x_e}{y_e - y} \tag{20}$$

where (x_e, y_e) is the coordinate of an epicentre in the xy plane from which all constant T_c lines emanate. x_e and y_e have values of 0.3320 and 0.1858, respectively. Clearly, n is the negative inverse slope of the line joining (x, y) with (x_e, y_e). The value of T_{cr}, as given by McCamy's formula, is

$$T_{cr} = 449\,n^3 + 3525\,n^2 + 6823.3\,n + 5520.33. \tag{21}$$

In the range of T_c from 2856 to 6500 K, McCamy's formula provides a maximum absolute error of 2 K, and is therefore, very accurate. Even for a wider range of 2000–12 500 K it is reasonably accurate. Equation (22) is a mapping from a real number n to another real number T_{cr}. The present method proposes to use two mathematically simple, yet very accurate, inverse mappings from T_{cr} to n. One will be used for $T_{cr} \le T_{c0}$, while the other for $T_{cr} > T_{c0}$, where T_{c0} is the value of the CCT for the source S_1.

Equation (20) can be rearranged as the equation of a straight line given, in slope–intercept form, by

$$y = -\frac{1}{n}\,x + \left(\frac{x_e}{n} + y_e\right). \tag{22}$$

We observe that for a fixed n, a fixed T_{cr} can be obtained from (21) and such a value of T_{cr} is obtained anywhere on the line given by (22). This line is therefore called an isotherm or an isoCCT line. Fig. 2 shows two isoCCT lines PQ_1 and PQ_2, corresponding to T_{cr} = 10 000 K and 2500 K, respectively.

In the range $(0.075 \le n < 0.725)$, or, equivalently, $(6052\ \text{K} \le T_{cr} < 12\,491\ \text{K})$, McCamy's formula can be closely fitted by a quadratic equation of the form:

$$an^2 + bn + c = 0 \tag{23}$$

where

$$a = 4064; b = 6640; c = 5536 - T_{cr}. \tag{24}$$

Similarly, in the range $(-0.68 \le n < 0.12)$, or, equivalently $(2369\ \text{K} \le T_{cr} < 6390\ \text{K})$, the quadratic equation (24) has coefficients

$$a = 3148; \quad b = 6766; \quad c = 5524 - T_{cr}. \tag{25}$$

The advantage of replacing the original McCamy's formula by two piecewise quadratic equations is that, for a given T_{cr}, a closed-form solution for n can be easily obtained from (23) and (24), or (23) and (25), depending on the range of T_{cr}. The closeness of the fits are verified by worst-case deviation in T_{cr} of 5 and 10 K, for (–0.68 ≤ n < 0.12) and (0.075 ≤ n < 0.725), respectively, from that given by McCamy's formula.

Once n is known from (23), we can find (x_b, y_b), the chromaticity coordinates of the intersection of two straight lines given by (18) and (22). This (x_b, y_b) coordinate pair produces the desired T_c and can be generated by mixing light fluxes from S_1 and S_2 using a blending ratio $r_D = D_2/D_1$.

The intersection points lie within the hollow rectangular boxes shown in Fig. 2. The solution for x_b, obtained from substitution of x by x_b and y by y_b in (18) and (22), is given by

$$x_b = \frac{x_e + n\,(y_e - y_2 + mx_2)}{mn + 1}. \tag{26}$$

Substitution of (26) into (17) yields r_a, from where r_D can be calculated using (16).

Computation of the individual values of D_1 and D_2 is rather straightforward considering the fact that the total required illuminance E_r on the work plane is the sum of the illuminance contributions E_1 and E_2

$$E_r = E_1 + E_2. \tag{27}$$

Substitution of (8), (9), (13), and (14) into (27) finally yields

$$D_1 = \frac{Er}{E_{M1}\,(1 + r_D\,r_E)}. \tag{28}$$

D_2 is determined from (15) as

$$D_2 = r_D D_1. \tag{29}$$

The values of the controlled outputs of the CCT and illuminance controller should ideally be the two duty cycles D_1 and D_2. But since D_1 and D_2 are two real numbers in general, they can not be directly transferred to the PWM registers of a microcontroller. The have to be converted to integers by the expessions as follows:

$$p_k = \text{round}\left(D_k.2^N\right) - 1, \quad k = 1, 2 \tag{30}$$

where *N* is the word length of the PWM registers. It is clear that the actual values of the duty cycles are not D_1 and D_2, in general, but $(p_1 + 1)/2^N$ and $(p_2 + 1)/2^N$. Consequently, the actual value of r_D is modified to $(p_2 + 1)/(p_1 + 1)$. This causes a quantization error and its effect on system performance will be examined in Section IV. The notion of a transition value D_{Tk} may be introduced here. The transition value of D_k is a value D_{Tk} such that, if for $D_k = D_{Tk}^-, p_k = p$, for $D_k = D_{Tk}+, p_k = p + 1$. This implies a step discontinuity in the transformation. An expresion for D_{Tk} can be derived from (30) to be

$$D_{Tk} = (p_k + 1.5)/2^N. \tag{31}$$

In summary, the control system, which is digital and algebraic in nature, accepts two reference inputs E_r and T_{cr} and depending on the chromaticity coordinates and luminance of the two sources—collectively termed as luminous parameters in this study—decides the selection of the color of the companion source S_2 in the form of a binary variable BLU_ON and calculates two more integer outputs p_1 and p_2. It should be noted here that the luminous parameters are not constants but are functions of their respective junction temperatures. However, the controller sample time *T* is small compared to the rise time of the junction temperatures corresponding to small step changes in *D*s that may occur between two consecutive cycles. This validates the assumption that the values of the luminous parameters are constants over a sampling period. A method for estimating the luminous parameters in every sample interval at runtime is presented in the next section.

C. Runtime Estimation of Luminous Parameters

A runtime estimation of the luminous parameters E_M, x and y of each LED requires an *a priori* knowledge of the variation of the parameters as functions of their respective junction temperatures. One-time, offline measurement and evaluation of some model parameters, discussed next, are necessary for the purpose.

The system hardware has been designed in such a way that the average value of forward drop of each LED, fed by a constant amplitude, constant frequency, variable pulse-width current, is connected to one channel of an on-chip ADC of the CICU. The average forward voltage of a particular LED u_{fa} is a function of its duty cycle *D* and its junction temperature θ_J. The output of the ADC n_a being directly proportional to u_{fa} can be expressed as

$$n_a = n_a\left(D, \theta_J\right). \tag{32}$$

An experiment is now conducted in which the values of n_a are recorded for two different ambient temperatures of 27 ± 2 and 40 ± 2 °C and at three values of $D = 0.1$, 0.5 and 0.9 for white LED, and $D = 0.1$, 0.35, and 0.6 for red and blue LEDs. The higher ambient temperature is usually taken as the maximum operating ambient temperature of the lamp. For brevity, the lower ambient temperature condition will be termed as the S (or, "standard ambient") condition and the higher ambient temperature condition will be termed as the H (or, "high ambient") condition. Symbols like $\psi|$S or $\psi|$H will denote the value of a variable ψ under standard ambient condition or high ambient condition, respectively. Each n_a is then expressed as a quadratic expression in *D* of the form

$$n_a = A_0 + A_1 D + A_2 D^2. \tag{33}$$

The values of the constants A_0, A_1, and A_2 under S and H conditions for the three LEDs are shown in Table I.

For the white LED, a plot of (33) for a limited range of *D* is shown in Fig. 3. We take $D = 0.6$ as an example and show $n_a|$S and $n_a|$H by points A and B, respectively, in Fig. 3. The values of $n_a|$S and $n_a|$H can be determined by using (33) along with appropriate values of A_0, A_1, and A_2 given in Table I. Actual value of n_a measured at runtime for the same *D* and shown by

TABLE I
EXPERIMENTALLY EVALUATED POLYNOMIAL COEFFICIENTS OF ADC OUTPUT FOR THE THREE LEDS

Colour →	White			Red			Blue		
Ambient temperature, °C↓	A_0	A_1	A_2	A_0	A_1	A_2	A_0	A_1	A_2
27 ± 2	9.39	979	−27.2	2.86	683	−21.5	7.4	905	−16.9
40 ± 2	9.01	962	−24.9	2.97	657	−15.5	6.45	890	−15.9

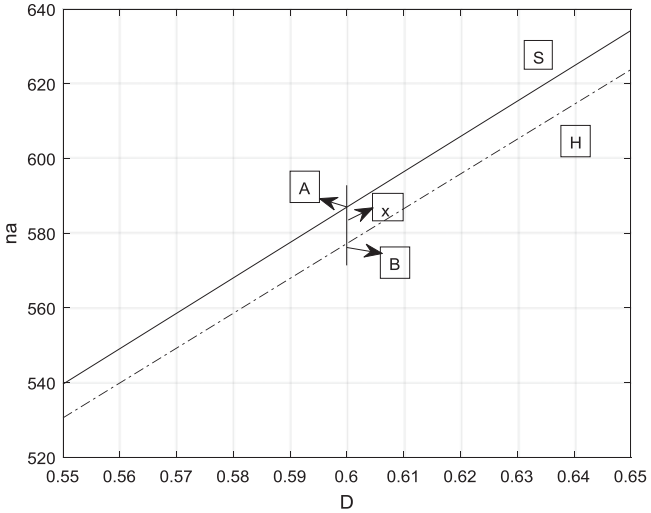

Fig. 3. Graphs showing plot of (33) at two different ambient temperatures.

TABLE II
EXPERIMENTALLY EVALUATED INTERCEPT AND SLOPE VALUES FOR WHITE LED

Ambient temperature, °C	$E_M(0)$, lx	m_{EM}, lx	x (0)	m_{x}	y (0)	m_y
27 ± 2	150.8	−9.256	0.3222	−3.6047E–3	0.3342	−5.4651E–3
40 ± 2	140.9	−10.95	0.3172	−4.6512E–3	0.3273	−6.2791E–3

TABLE III
EXPERIMENTALLY EVALUATED INTERCEPT AND SLOPE VALUES FOR RED LED

Ambient temperature, °C	$E_M(0)$, lx	m_{EM}, lx	x (0)	m_x	y (0)	m_y
27 ± 2	72.8	−10.35	0.6919	2.2093E–3	0.3072	−1.8605E–3
40 ± 2	56.2	−10.35	0.6954	1.7742E–3	0.3035	−1.3953E–3

TABLE IV
EXPERIMENTALLY EVALUATED INTERCEPT AND SLOPE VALUES FOR BLUE LED

Ambient temperature, °C	$E_M(0)$, lx	m_{EM}, lx	x (0)	m_x	y (0)	m_y
27 ± 2	6.77	−0.5116	0.1391	−1.1628E–4	0.0342	1.2791E–3
40 ± 2	6.71	0.093	0.1390	−3.4884E–4	0.0381	9.3023E–4

point X, may be, in general, different from either of them. We, therefore, define a variable d given by

$$d = (n_a|\mathrm{S} - n_a)/(n_a\,|\mathrm{S} - n_a|\,\mathrm{H})\,. \tag{34}$$

As will be shown, this variable d, which is the ratio of the lengths of the line segments AX and AB, plays an important role in determining the values of the luminous parameters. Experiments have shown that the parameters very nearly follow the equations of straight lines given in slope–intercept form by

$$E_M\,(D)\,|\mathrm{S} = E_M\,(0)|\,\mathrm{S} + m_E|\mathrm{S}.D \tag{35a}$$

$$E_M\,(D)\,|\mathrm{H} = E_M\,(0)|\,\mathrm{H} + m_E|\mathrm{H}.D \tag{35b}$$

$$x\,(D)\,|\mathrm{S} = x\,(0)|\,\mathrm{S} + m_x|\mathrm{S}.D \tag{36a}$$

$$x\,(D)\,|\mathrm{H} = x\,(0)|\,\mathrm{H} + m_x|\mathrm{H}.D \tag{36b}$$

$$y\,(D)\,|\mathrm{S} = x\,(0)|\,\mathrm{S} + m_y|\mathrm{S}.D \tag{37a}$$

$$y\,(D)\,|\mathrm{H} = x\,(0)|\,\mathrm{H} + m_y|\mathrm{H}.D. \tag{37b}$$

The slope and the intercept parameters from (35a) to (37b) can be determined from the values of the left-hand sides for two extreme values in the working range of D (0.1 and 0.9 for white LED and 0.1 and 0.6 for the companion LEDs). Caution is taken so that a dependent variable reaches its steady state before recording its value. The values of the parameters so obtained are given in Tables II–IV. The evaluation of the present 12 slope and intercept constants and the earlier six constants $A_0|\mathrm{S}, A_1|\mathrm{S}, A_2|\mathrm{S}, A_0|\mathrm{H}, A_1|\mathrm{H}$ and $A_2|\mathrm{H}$ for each LED, although done offline and only once, is time consuming and therefore, adds to the system cost.

In the discussions to follow we shall, for the sake of brevity, use a common variable φ to indicate the the luminous parameters because each will be estimated in the same manner at the runtime and the meaning of φ will become clear from the context. Since the value of duty cycle D is constant over a sampling period of the controller, each φ is a function of n_a only and assuming further that each such function is continuous in the interval $(n_a|\mathrm{S}, n_a|\mathrm{H})$, any φ for a given n_a can be determined by the linear interpolation formula

$$\varphi = \varphi\,|\mathrm{S} - (\varphi|\,\mathrm{S} - \varphi\,|\mathrm{H})/(n_a|\,\mathrm{S} - n_a\,|\mathrm{H}).(n_a|\,\mathrm{S} - n_a). \tag{38}$$

In view of the variable d defined earlier in (34), (38) simplifies to

$$\varphi = \varphi\,|\mathrm{S} - (\varphi|\,\mathrm{S} - \varphi|\mathrm{H}).d. \tag{39}$$

Replacing φ by the required luminous parameter $E_M\,, x$ or y in (39), these parameters for the two active LEDs are estimated at runtime. If the LEDs are operated at lower ambient temperature than that under S condition, the value of n_a will be higher than $n_a|\mathrm{S}$ and d will become negative. Although (38) and (39) are still valid, the actual mathematical process becomes one of linear extrapolation rather than that of linear interpolation.

Once the values of the luminous parameters are estimated, the remaining calculations for determining the controller outputs, as described in the previous section, are rather straightforward. The algorithmic steps are given in a flowchart form in Section III.

Fig. 4 shows the variation of the estimated and measured luminous parameters of the white and the red LEDs at different heatsink temperatures. The normalized values of parameters have been obtained by dividing the actual value with that of the same at 30 °C. It is observed that the peak illuminance decreases with temperature for both the LEDS.

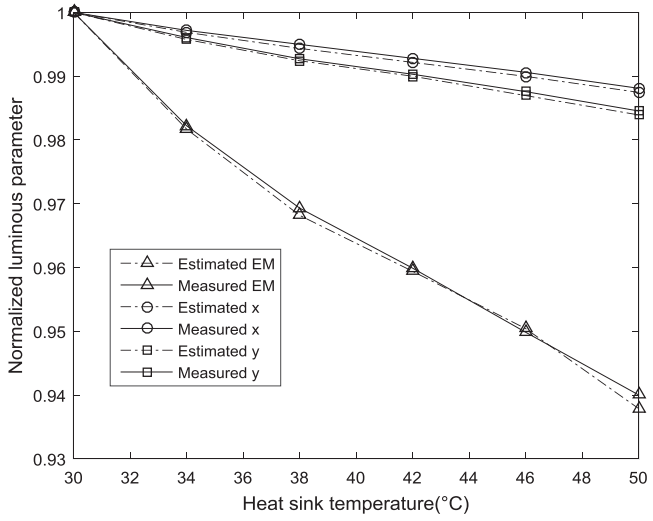

(a)

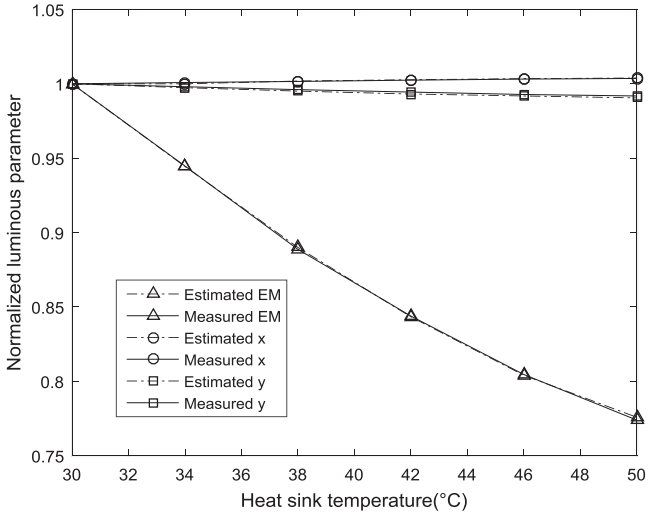

(b)

Fig. 4. Normalized luminous parameters of the LEDs as a function of heatsink temperature. (a) White. (b) Red.

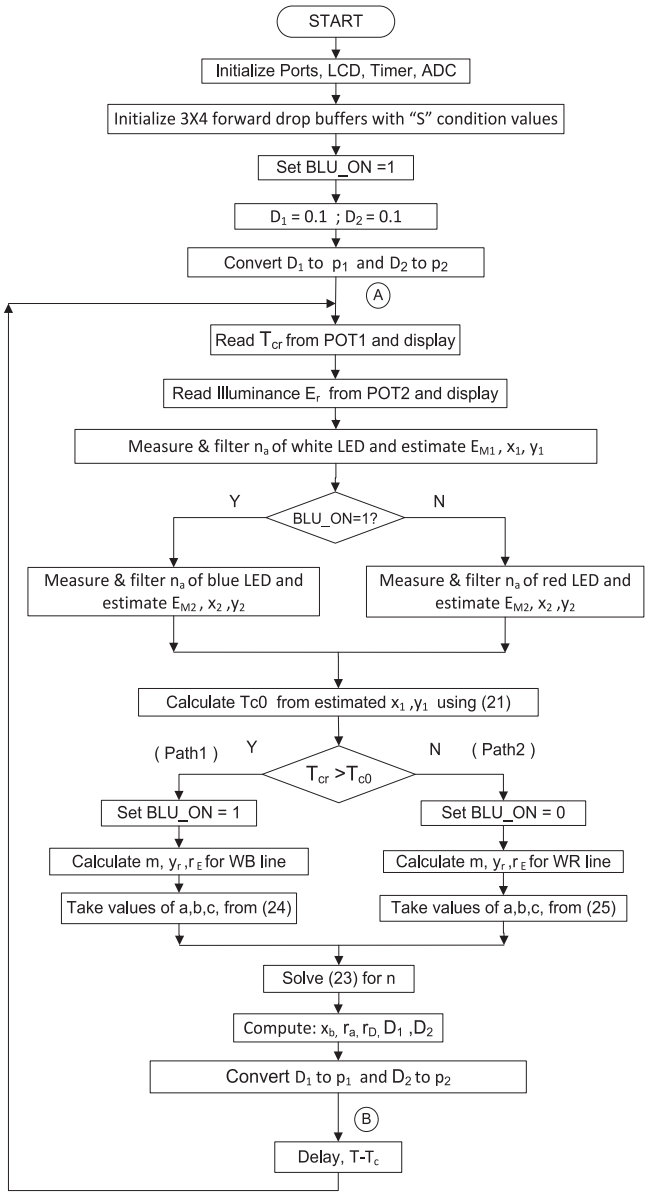

Fig. 5. Flowchart of the proposed CCT and illuminance control algorithm.

III. Features of the CCT and Illuminance Control System

A. Software Features of the CICU

The computational algorithm for the CICU is shown in the flowchart of Fig. 5, where the numbers in parenthesis indicate the equation numbers. The controller outputs BLU_ON, p_1 and p_2, are generated in every sampling period T of the system. The calculations can be broadly divided into two groups: the aperiodic or once-only type and the periodic or inside-the-loop type. The fixed calculations, which do not depend on the reference inputs T_{cr} and E_r, are kept in the aperiodic group. The buffers mentioned in the third block from top are used for digital, low-pass, moving-average filtering of ADC outputs n_a mentioned earlier in Section II-C. The branching in the loop to paths 1 and 2 occurs due to different values of parameters shown for WB and WR blending lines, respectively. The paths 1 and 2 finally merge together and the remaining common calculations are then made. The average value of the code execution time T_c from nodes A to B decides the delay time T_d according to the equation

$$T_d = T - T_c. \tag{40}$$

For the ATmega32A microcontroller, [38] used in the CICU, running at a clock frequency of 12 MHz, the average value of T_c is about 5.5 ms. Thus, a delay time of 994 ms will produce the desired sampling period of 1 s.

The human interface of the system is extremely simple. The CCT and illuminance set points are supplied to the system in a convenient form using two analog voltages from two potentiometers, POT1 and POT2, respectively. The CCT can be set in the range of 2500–12 500 K, with a resolution of 100 K and an illuminance in the range of 5–120 lx, with a resolution of 1 lx.

Both of these data are displayed on a common liquid crystal display (LCD).

B. Hardware Features of the Proposed System

1) CICU: The main tasks of the CICU have already been mentioned. The CICU comprises of an ATmega32A MCU, a common JHD162A, 16 × 2 LCD display, a DEMUX using a CD4011 CMOS quad, two-input NAND gate and two linear 10-K POTs. Any other MCU, irrespective of the manufacturer, having at least five ADCs, two 10-bit resolution PWM channels, 8 KB of flash memory and eight programmable I/O lines, could also be used to implement the proposed CICU. To avoid visible flicker, it has been customary to use a PWM frequency of more than 100 Hz [39], [40]. However, a recent IEEE Standard, 1789-2015 [41] recommends that the PWM dimming frequency should be higher than 1.25 kHz. Also, at this frequency and above, there is no restriction on modulation percentage of the PWM dimming. We have used a frequency of 1.46 kHz, a value that is easily programmable for the aforementioned MCU operating at a clock frequency of 12 MHz, for both the 10-bit PWM channels.

The DEMUX shown in Fig. 1 is implemented using a common quad, two-input, NAND CMOS IC CD4011. Depending on the state of the select line BLU_ON, the DEMUX will drive the red LED or the blue LED string from PWM2 channel. If BLU_ON is high, the PWM signal generated at the PWM2 channel of the MCU is steered to A_1 to drive the blue LED string. On the other hand, if BLU_ON is low, the PWM signal is steered to A_0 to drive the red LED string. The PWM1 channel of the MCU is used to drive the white LED string.

2) Constant Voltage Switched-Mode Power Supply (SMPS): As the primary source is normally an ac line at power frequency, an ac–dc converter is needed to supply the current to the LED strings. The control of current amplitude to the individual strings is done by constant-current drivers described in the next section. In our case, an SMPS has been designed using flyback topology to provide a constant voltage of 12 V and an output current of 2 A.

The self-oscillating flyback converter, also known as the ringing-choke converter (RCC), is a popular circuit for cost-sensitive, low-power, offline applications [42], [43]. The noted advantage of an RCC of this type is that it can be implemented with very few discrete components. A detailed design-oriented steady-state analysis and a small-signal model of the self-oscillating flyback converter have been provided in the above references. The pulse-width modulator and the switch driver are implemented by using a single transistor, a positive feedback winding, and a resistor divider network. In our case, tight voltage regulation is not required, because LEDs are driven by their individual constant current drivers. Thus, a simple feedback control may be implemented by using a single zener diode and an optocoupler. The +5-V supply required by the MCU, the LCD, and the DEMUX is obtained from a LM7805 linear regulator fed from the 12-V supply.

3) PWM Dimmable High-Side LED Driver: A TTL-logic controllable, high-side, constant peak current LED driver has been designed to drive the LED strings. The circuit diagram of a typical driver is shown in Fig. 6. When the logic control input LED_ON is 1, the LEDs turn on at a programmed value of peak current decided by $R_{\rm CS}$, the value of the current sensing resistor *R*4. On the other hand, for LED_ON = 0, the LEDs are OFF. The LED_ON signals, depending on the LED to be driven, are the PWM outputs obtained either from the MCU (for white LED) or from the DEMUX (for red or blue LED). An explanation of the operating principle of the driver follows.

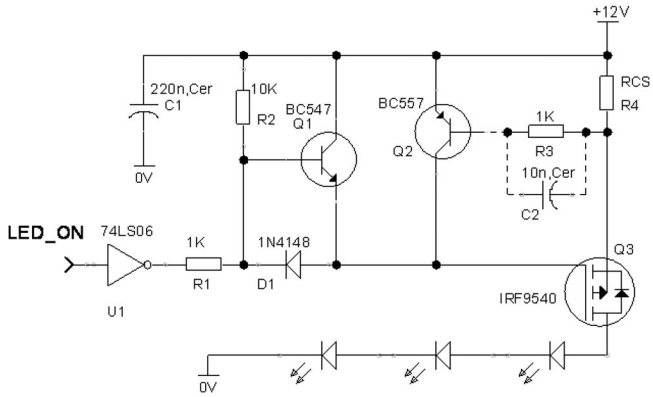

Fig. 6. High-side constant current LED driver.

For logic input 0, the output of the TTL open-collector inverter U1 goes to Hi-Z state and the transistor Q1 goes to linear mode with a low value of collector-to-emitter voltage $U_{\rm CE}$ slightly greater than its base-to-emitter voltage $U_{\rm BE}$. As a result, the magnitude of gate-to-source voltage $U_{\rm GS}$ of the output P-channel MOSFET Q3 goes below its threshold level. Q3 thus turns off, resulting in zero current through the LED string. Since the drop $U_{\rm CS}$ across the current sensing resistor *R*4 is zero, the PNP transistor Q2 remains cut-off and does not affect the operation of the circuit.

Corresponding to a logic input of 1, the output voltage of the inverter goes close to ground and the effective gate-to-source capacitance $C_{\rm GS}$ of Q3 starts to get charged. Q1 turns off now due to reverse biasing of its base–emitter junction caused by forward current flow in *D*1. When the resulting magnitude of $U_{\rm GS}$ crosses the threshold, the source current of Q3, which is also equal to the LED current $I_{\rm LED}$, starts to increase. This increase of $I_{\rm LED} = I_S$ does not take place indefinitely but instead is limited to a value at which $U_{\rm CS}$ equals the base–emitter threshold voltage $U_{T,\rm BE}$ of Q2. Any increase of $I_{\rm LED}$ causes an increase in the base current of Q2 resulting in drop of magnitude of its $U_{\rm CE}$, which is also the magnitude of $U_{\rm GS}$ of the MOSFET. This restores the value of $I_{\rm LED}$, provided the current control loop is stable. The preceding discussions, under the assumption of stability, give an expression for $I_{\rm LED}$ as follows:

$$I_{\rm LED} = U_{T,\rm BE}/R_{\rm CS}. \tag{41}$$

The current control loop has a very high low-frequency loop gain and, if the voltage $U_{\rm CS}$ is directly coupled to the base of Q2 through a resistor *R*3 alone, causes an instability in the form of a high frequency oscillation in $I_{\rm LED}$. A common remedy in the form of putting a lead network in the feedback path works in

TABLE V
IMPORTANT PARAMETERS OF THE LED AND ITS DRIVER CIRCUIT

LED color	Power rating of each LED (W)	Number of LEDs in series	$R_{\rm CS}$ (Ohm)	$I_{\rm LED-Pk}$ (mA)	Approximate peak *E* at work plane, lx
White	1	3	1.9	316	146
Red	1	3	2.2	275	68
Blue	1	3	5.6	108	6.5

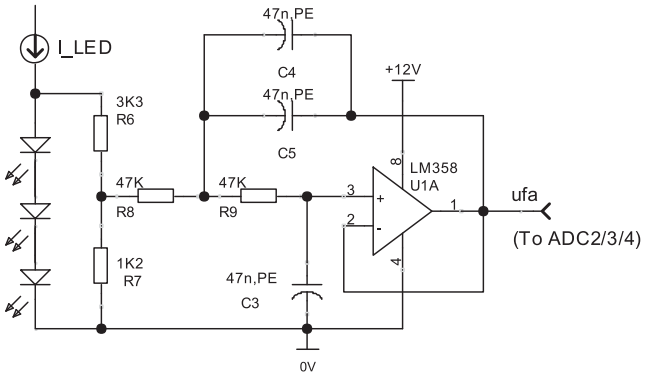

Fig. 7. Second-order Butterworth LPF.

this case. It was realized by shunting the resistor *R*3 by a 10-nF capacitor *C*2.

The change in the output LED current in response to the logic control signal cannot be instantaneous—instead there are finite turn-on and turn-off delays of $t_{d\rm on}$ and $t_{d\rm off}$, respectively. Experimentally, it was found that $t_{d\rm on}$ and $t_{d\rm off}$, respectively, have values of 3.5 and 1 μs. Since $t_{d\rm on} > t_{d\rm off}$, the output pulse width will become less than the input one by an amount of $(t_{d\rm on} - t_{d\rm off})$. This is circumvented by adding a correction term in *D*, whose value is $(t_{d\rm on} - t_{d\rm off})/T_{\rm PWM}$, where $T_{\rm PWM} =$ 683 μs is the time period of the PWM drive signal.

The values of $R_{\rm CS}$ and the corresponding current amplitudes along with some other parameters are shown in Table V. The data in the sixth column are calculated from the average illuminance for $D = 0.5$.

4) LED Average Forward Drop Measurement Circuit: The instantaneous forward voltage across a series-connected LED string is a periodic rectangular pulse with a time period $T_{\rm PWM}$, a duty cycle *D*, and an amplitude that is the sum of the forward drops of the LED at the constant level of peak current. A fraction of this voltage, decided by the attenuation ratio *R*7/(*R*6 + *R*7), when given to a low-pass filter (LPF) with a proper lower cut-off frequency will produce an output with a dc component $u_{\rm fa}$ along with a negligible ripple. The circuit diagram of the attenuator and the LPF is shown in Fig. 7. The output of the LPF is finally converted by the respective on-chip ADC to an integer n_a given by

$$n_a = \text{round } (u_{\rm fa}/U_{R,\rm AD}) .2^{\rm Nad} \tag{42}$$

where $U_{R,\rm AD}$ is the reference voltage and Nad is the number of bits, respectively, of the ADC. n_a is also, by design, internally clamped to an upper limit of $2^{\rm Nad} - 1$. The input attenuator is so chosen that full input range of the ADC is utilized ensuring that the maximum value of $u_{\rm fa}$, corresponding to $D = 1$, does not exceed $U_{R,\rm AD}$, which has a value of 2.56 V in our case.

A second-order Butterworth LPF was used in our implementation and its lower cut-off frequency was chosen to be 1/20th that of the input fundamental frequency of 1.46 kHz. For the standard component values used, the lower cut-off frequency turns out to be 72 Hz, a value very close to the design target.

A further filtering of the ripple is effected by taking four samples of the ADC output at intervals of $T_{\rm PWM}/4$ or, approximately 170 μs and taking the average of four resulting values of n_a. Although this effectively increases the ADC conversion time to $T_{\rm PWM}$, it is, since $T_{\rm PWM} << T_c$, of no serious concern.

5) Arrangement of the LEDs: A primitive arrangement of the LEDs was done in the prototype to meet the basic optical and thermal requirements. To facilitate adequate color mixing, free of color patches, the LEDs were placed in such a way that

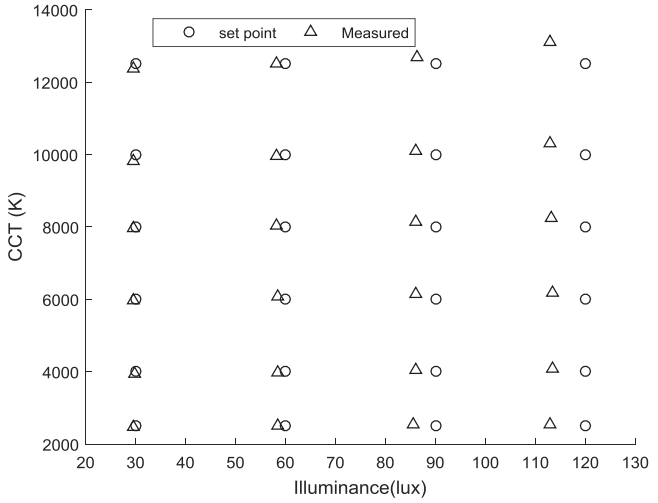

Fig. 8. CCT and illuminance measurement at 27 °C (fixed luminous parameters).

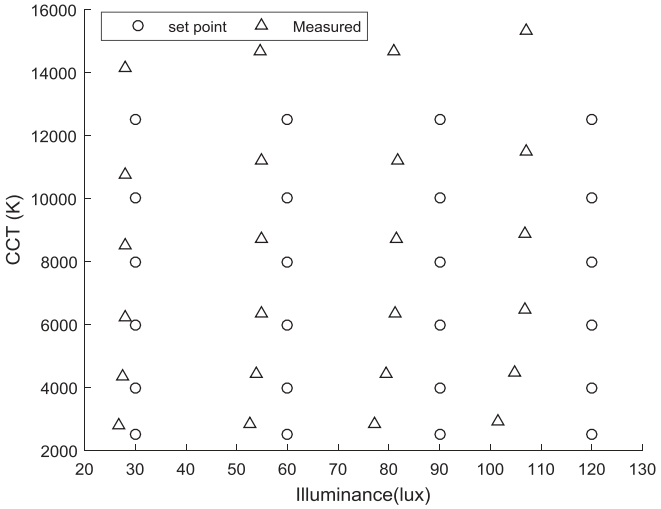

Fig. 9. CCT and illuminance measurement at 45 °C (fixed luminous parameters).

TABLE VI
ERROR PERFORMANCE INDICES OF THE SYSTEM WITH FIXED LUMINOUS PARAMETERS

Ambient temperature (°C)	RMS error in T_c (K)	RMS error in E (lx)	Maximum absolute error in T_c (K)	Maximum absolute error in E (lx)
27 ± 2	172.2	4.09	610 at $T_{cr} = 12\,500$ K; $E_r = 120$ lx	7.2 at $T_{cr} = 12\,500$ K; $E_r = 120$ lx
45 ± 2	1148.4	9.28	2810 at $T_{cr} = 12\,500$ K; $E_r = 120$ lx	18.5 at $T_{cr} = 2500$ K; $E_r = 120$ lx

the distance between the farthest LEDs was small compared to the distance of the assembly from the work plane. The centers of the three CW-PC LEDs constituting the main source S_1 were located equally spaced on a pitch circle of diameter 40 mm. The six companion red and blue LEDs were placed alternately so that their centers were on a concentric circle of 80 mm diameter with two consecutive LEDs making an angle of 60° at the center. The heatsink was a 1.6-mm-thick-circular aluminum plate 110 mm in diameter. At the maximum light output level, the temperature rise of the heatsink center was only approximately 8 °C above the ambient.

IV. EXPERIMENTAL RESULTS AND OBSERVATIONS

A. Performance of the CCT and Illuminance Control System

The system was first operated with fixed luminous parameters measured at $D_1 = 0.5$ and $D_2 = 0.35$ for the main and companion LEDs, respectively. Twenty-four different combinations, corresponding to four values of values of E_r (30, 60, 90, and 120 lx) and six values of T_{cr} (2500, 4000, 6000, 8000, 10 000, and 12 500 K) at each E_r are set for measuring the CCT and E errors. The readings of the photometric quantities have been taken by using a Konica-Minolta CL200A Chroma Meter which was used for determining the LED parameters as described in Section II. The experimental plots of set point and measured values for ambient temperatures of 27 and 45 °C are shown in Figs. 8 and 9, respectively. Two performance indices, namely, RMS error and maximum absolute error, are also chosen to evaluate the system performance at these sample set point combinations. The results are shown in Table VI.

The results in Table VI show that the performance of the system, both in terms of RMS error and absolute error, for T_c and E are quite high, especially when one compares the corresponding figures for the compensated system to be considered next.

The system was next operated in temperature compensated mode using the parameter estimation algorithm discussed in Section II-C. The experimental results for ambient temperatures of 10, 27, and 45 °C are shown in Figs. 10, 11, and 12, respectively, in the form of scatter plots. The performance indices at different ambient temperatures are given in Table VII, where operation at a low ambient temperature of 10 °C has also been included. At the low temperature, the luminous parameters are estimated at runtime by extrapolation. Figs. 11 and 12, when compared with Figs. 8 and 9, exhibit much lower errors in CCT and E for the compensated system. A comparison of the results in Tables VI and VII clearly indicates the superiority of the compensated system over the uncompensated one. It also shows that the system can be operated over a wide ambient temperature excursion between 10 and 45 °C.

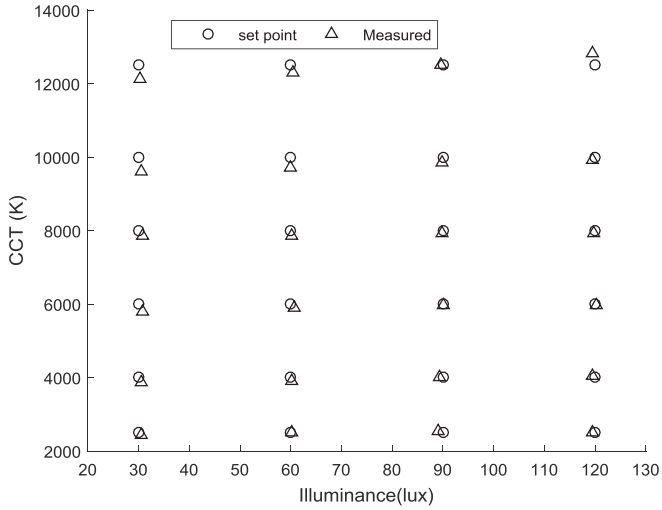

Fig. 10. CCT and illuminance measurement at 10 °C (runtime estimated parameters).

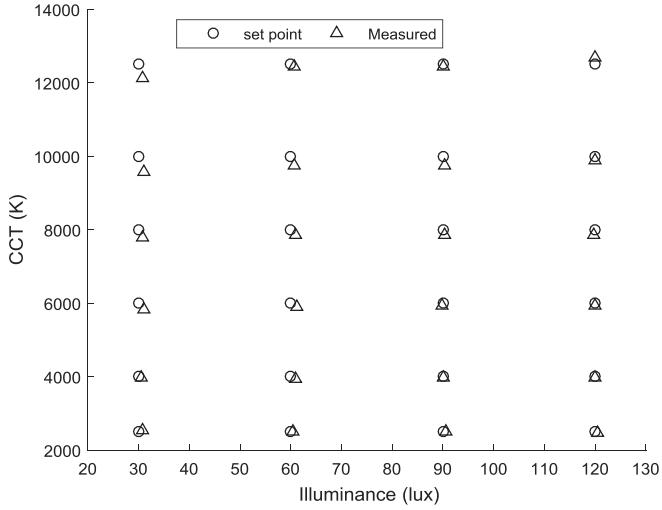

Fig. 11. CCT and illuminance measurement at 27 °C (runtime estimated parameters).

Maintaining the temperature compensated system at the standard ambient temperature of 27 ± 2 °C, the CCT and illuminace errors as functions of the set point CCT, at various illuminance set points were evaluated. The data are plotted in Figs. 13 and 14.

The following three plots show the internal functioning of the controller at an ambient temperature of 27 ± 2 °C. The ratio

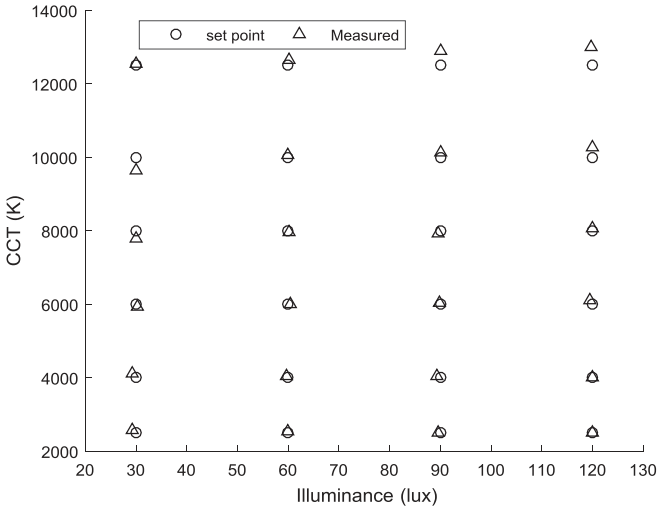

Fig. 12. CCT and illuminance measurement at 45 °C (runtime estimated parameters).

TABLE VII
ERROR PERFORMANCE INDICES OF THE SYSTEM WITH RUNTIME PARAMETER ESTIMATION

Ambient temperature (°C)	RMS error in T_c (K)	RMS error in E (lx)	Maximum absolute error in T_c (K)	Maximum absolute error in E (lx)
10 ± 2	167.5	0.46	286	0.8
27 ± 2	161.5	0.61	319	1.1
45 ± 2	167.2	0.31	400	0.8

r_a, which determines the position of x_b on the blending line, is plotted as a function of set CCT in Fig. 15. It is observed that r_a is not affected by the illuminance set point. Fig. 16 shows how the duty cycles D_1 and D_2 change with set CCT at two different values of set point E. It is apparent from this figure that the value of $r_D = D_2/D_1$ increases on both sides of $D_2 = 0$ point where the only source is S_1. In Fig. 17, the computed values of the luminance contributions $E_{M1} \cdot D_1$ and $E_{M2} \cdot D_2$ are plotted as functions of set CCT. It is obvious that at a different ambient temperature, while the values of the dependent variables in these three graphs will change, the shapes of the graphs will be retained.

The relative efficiency as functions of set CCT at 120 lx has been plotted in Fig. 18. The figure shows that for fixed lumen output the efficiency is decreasing for both RW and BW mixing as efficacy of companion LED is less than that of the white LED.

B. Measurement of D_{uv} and CRI

Although the requirements of a wide range of CCT and of illuminance have been met, the deviation of the locus of the operating points, namely the WB and WR line segments, from the Planckian locus is clearly visible. To quantify the deviation, a commonly used measure, D_{uv}, is used. The values of D_{uv} at selected values of CCT are computed by transformation of the CIE 1931 *xy* coordinates to the CIE 1960 *uv* coordinates system

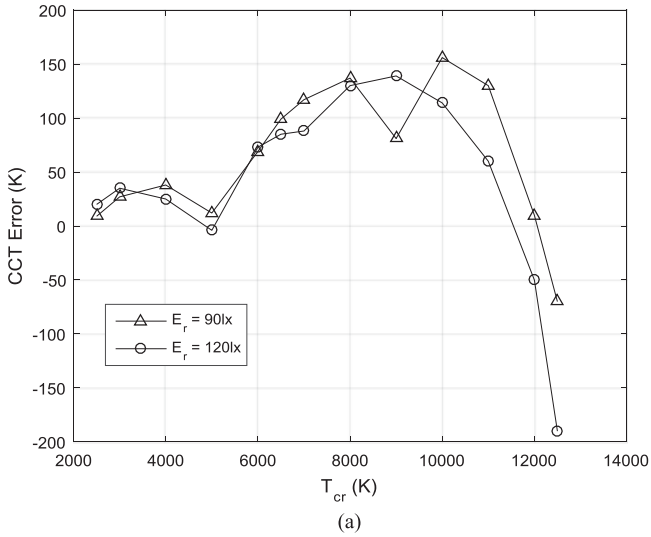

(a)

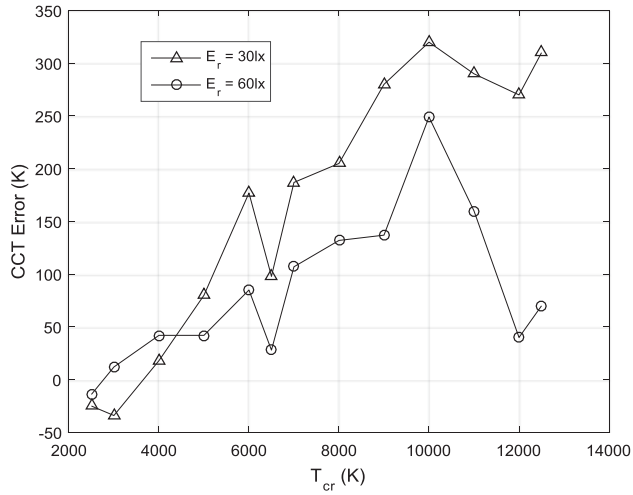

(b)

Fig. 13. Graphs showing the error in CCT as a function of set point CCT. (a) E = 120 lx and 90 lx. (b) E = 60 lx and 30 lx with runtime parameter estimation.

and subsequent evaluation of the linear distance between actual operating point and the corresponding point on the Planckian locus the in the *uv* plane. By definition, as the R-W-B locus is always below the Planckian locus, D_{uv} is negative for all the points. A plot of D_{uv} as a function of CCT is shown in Fig. 19. Studies conducted at National Institute of Standards and Technology (NIST, USA) [44] indicate that for a CCT range of 2700–6500 K, an approximate D_{uv} of -0.015 appeared to be most natural. For the CCT range of 2500–4000 K, our system has a larger magnitude of D_{uv}. A possible way to mitigate the problem is discussed at the end of this section.

To ascertain the color quality of the light produced by the system over the entire range of CCT at 120 lx, the full-scale value of the illuminance set point, the most common color rendition metric CRI R_a was used. It was measured by a Konica-Minolta CL-70F CRI-Illuminance meter. The values obtained are shown in Table VIII. For a CCT range of 4000–12 500 K, the value of CRI is more than 82, a figure that is often seen for many commercial quality, fixed CCT, LED lights. The reason for a

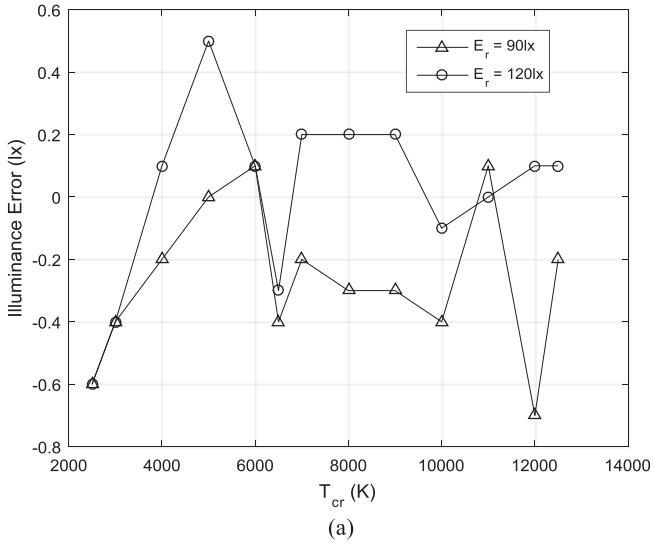

(a)

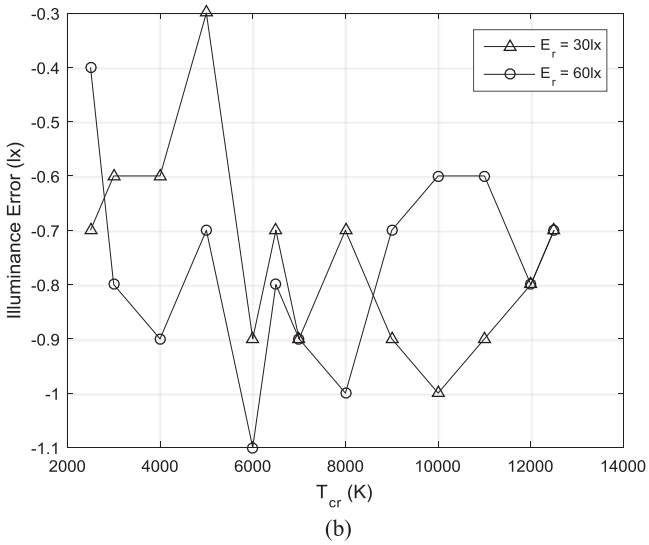

(b)

Fig. 14. Graphs showing the error in illuminance as a function of set point CCT. (a) $E = 120$ lx and 90 lx. (b) $E = 60$ lx and 30 lx with runtime parameter estimation.

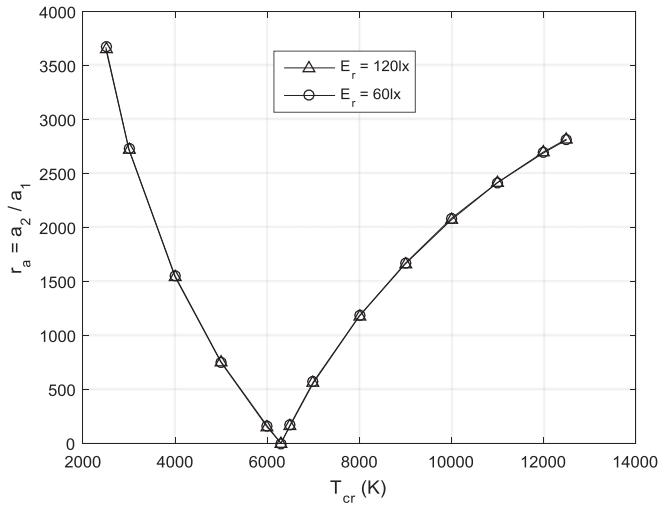

Fig. 15. Ratio r_a as a function of set CCT at 60 and 120 lx.

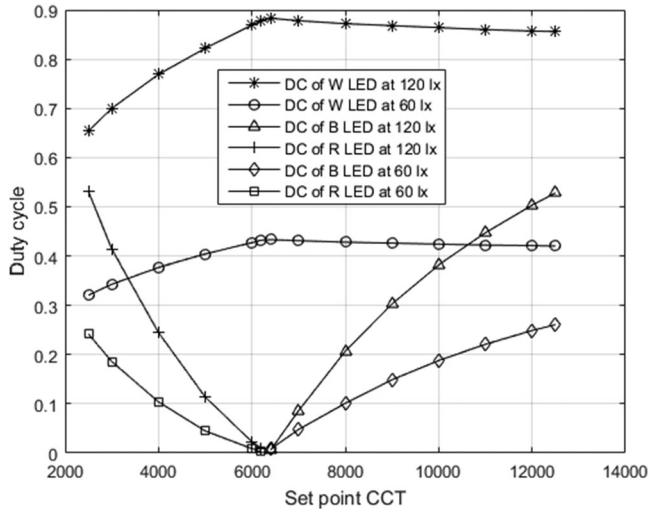

Fig. 16. D_1 and D_2 as functions of set CCT at 60 and 120 lx.

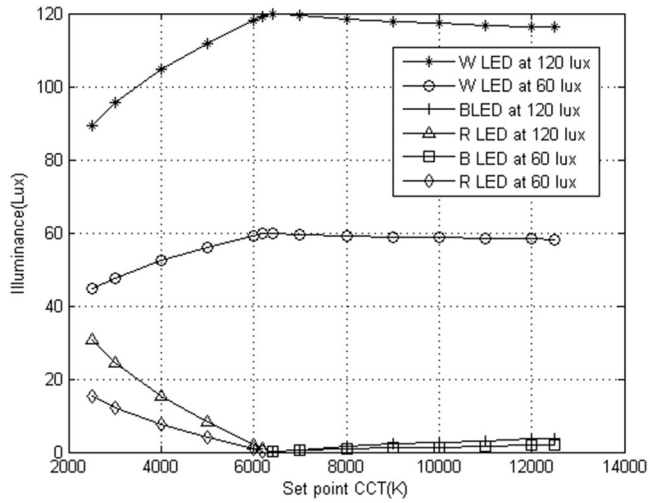

Fig. 17. Illuminance contribution from individual sources as functions of set CCT at 60 and 120 lx.

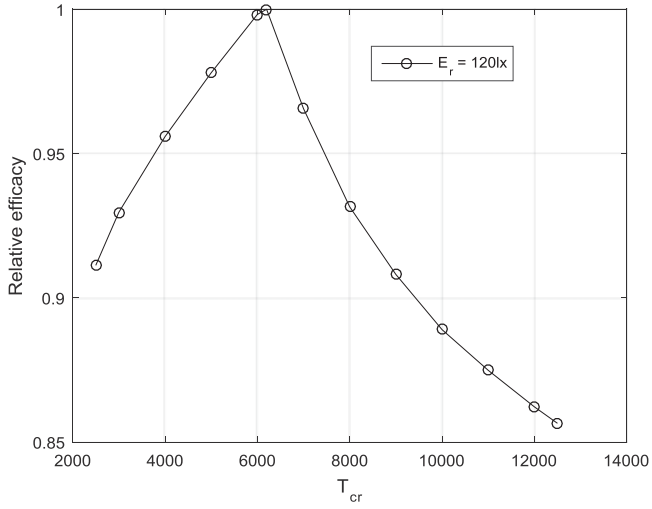

Fig. 18. Relative efficiency as functions of set CCT at 120 lx.

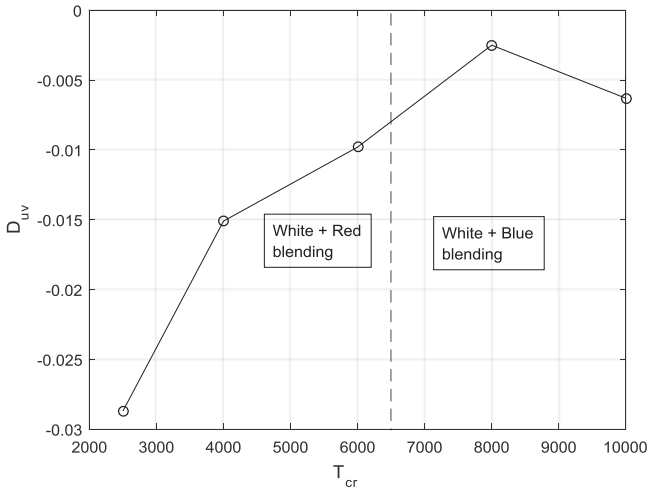

Fig. 19. Plot of experimental D_{uv} as a function of set point CCT.

fall of CRI for a CCT below 4000 K is the marked deviation of the WR blending line from the Planckian locus and an excessive red content in the mixed light. At the end of this section, we present a possible solution to this problem also.

Fig. 20 shows the spectral power distribution (SPD) of the proposed RBW LED lighting system at 4000, 5000, 6000, and 7000 K. Measured CRI at 6000–7000 K is found to lie in the band 88.3–90.1 as given in Table VIII. From the SPD curve, it has been found that the peaky nature in the red region is less for 6000–7000 K, which leads to a high CRI value in this region.

C. Observation Regarding Output Quantization Error

One of the major sources of error in CCT, as already pointed out in Section II-B, is the quantization of the controller output. Before presenting the observed effect, a little detailed exposition of the phenomenon is in order. One can, by use of (31), find two successive transition values of a particular *D*. For example, by setting $p = (47, 48, 49)$ the values of D_T obtained are 0.04736 and 0.04834 for the 47-to-48 and 48-to-49 transitions, respectively. Thus, for *D* in the range of (0.04736, 0.04834), *p* remains unchanged at 48. Consequently, the value of the duty cycle of the PWM drive signal remains unchanged and no control over *E* or CCT can be exercised. To demonstrate the effect of this output quantization, we had, with a goal of obtaining a CCT of 9200 K and an *E* of 30 lx, manually set the values of p_1 to 212 and 213, and p_2 to 48 and 49 and measured the CCT at the four possible combinations of p_1 and p_2. For our previously fixed value of $E_M\_B(0) = 6.77$ lx, the results are shown in Table IX. It is clear that the set CCT cannot be met in general due to the availability of a limited number of choices of the manipulated variables p_1 and p_2, resulting due to quantization. The last observation is true even when the controller works in automatic mode.

While selecting the peak LED current and the resulting peak illuminance for the blue LED shown in Table V, much lower values were chosen compared to those of the red LED. It was accepted that, due to the limited accuracy caused by the limited resolution of the luxmeter, the measurement of peak illuminance was subject to a large error. However, the range of the manipulated variable p_2 was about 0–120 giving a resolution of 1 in 120. The consequential quantization error has been demonstrated in Table IX. The error band in CCT for a fixed $p_1 = 210$ is 45 K. To see the effect of choice of the peak illuminance on quantization error, its value was raised to 12.07 lx and the same experiment was repeated. The results are reproduced in Table X. The range of the manipulated variable p_2 was about 0–60 giving a resolution of 1 in 60. As expected, the error band in CCT for a fixed $p_1 = 212$ increases to 117 K. It is thus concluded that a tradeoff between possible error in measuring E_M for the least contributing S_2 (blue LED in the present case) and the resulting quantization error must be made.

D. Comparison of the Proposed LED Lighting System With ANSI Standard

The ANSI standard C78.377A-2008 [45] for the chromaticity of solid-state lighting products is reproduced in Table XI for ready reference. Form Fig. 21, it is observed that the CCT tolerance requirement is satisfied for both the CCTs for all the values of set illuminances. The D_{uv} values for WR line, which are not plotted in Fig. 22, are always negative and higher than the ANSI specified values. On the other hand, from the D_{uv} values for WA (white-amber) blending plotted in Fig. 22, it is observed that the D_{uv} is within the specified range for 3700–6200 K. The ANSI C78.377 standard state that the tolerance range specified in Table XI is applicable for indoor lighting; higher tolerance values are often acceptable for other applications.

The expression for the ΔT and D_{uv} of Table XI for the flexible CCT have been given in the specified standard [45]. In accordance with the standard, the maximum and minimum tolerance range of CCT and D_{uv} have been plotted in Figs. 21 and 22, respectively.

E. Improvement of D_{uv} and CRI

To improve the value of D_{uv} value for CCTs lower than that of S_1, the red LED source can be replaced by a source, say *T*, such that the blending line WT, as shown in Fig. 2, is closer to the Planckian locus. In an initial trial, the red LED was replaced by an amber LED whose measured *xy* coordinates under 'S' condition and a duty cycle of 0.1 were 0.5685 and 0.4295, respectively. The peak current value was kept the same as that of the red LED. The value of D_{uv} at 2500 K had remarkably improved to -0.007. However, the spectral response characteristic of the amber LED had a negligible red content as observed by the Konica-Minolta CL-70F CRI-Illuminance meter. Owing to this, the value of CRI in the 2500–4000 K band cannot be improved by the use of this LED. Therefore, no further results were collected.

Currently, work is in progress with a red–green composite source for S_2. As the number of drivers has to be limited to 3, the series string of three red LEDs is replaced by a string of two red LEDs and a green LED (R + G + R). The series connection ensures that the same instantaneous current passes through all the LEDs and that they have the same duty cycle. As the *xy* coordinates of the composite source depend on those of

TABLE VIII
CRI MEASUREMENT

Set CCT	2500	3000	4000	5000	6000	6200	6400	7000	8000	9000	10 000	11 000	12 000	12 500
Measured CRI	71.3	74.0	82.4	86	90.1	90.3	90.5	88.3	84.8	84.2	84.2	84.1	84.1	84.0

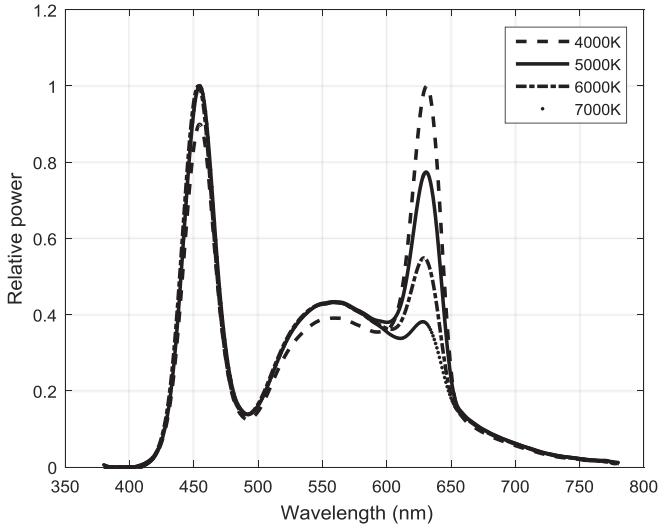

Fig. 20. SPD of CCT (4000, 5000, 6000, and 7000 K).

TABLE IX
CCT VALUES (K) AT DIFFERENT VALUES OF p_1 AND p_2

$p_1 \rightarrow$ $p_2 \downarrow$	210	211
94	9192	9157
95	9237	9210

EM_B ($D = 0$) = 6.77 lx.

TABLE X
CCT VALUES (K) AT DIFFERENT VALUES OF p_1 AND p_2

$p_1 \rightarrow$ $p_2 \downarrow$	212	213
48	9140	9122
49	9257	9233

EM_B ($D = 0$) = 12.07 lx.

TABLE XI
ANSI C78.377A STANDARD FOR CHROMATICITY SPECIFICATIONS

Nominal CCT (K)	Target CCT and tolerance (K)	Target D_{uv} and tolerance
2700	2725 ± 145	0.000 ± 0.006
3000	3045 ± 175	0.000 ± 0.006
3500	3465 ± 245	0.000 ± 0.006
4000	3985 ± 275	0.001 ± 0.006
4500	4503 ± 243	0.001 ± 0.006
5000	5028 ± 283	0.002 ± 0.006
5700	5565 ± 355	0.002 ± 0.006
6500	6530 ± 510	0.003 ± 0.006
Flexible CCT (2700–6500 K)	$T \pm \Delta T$	$D_{uv} \pm 0.006$

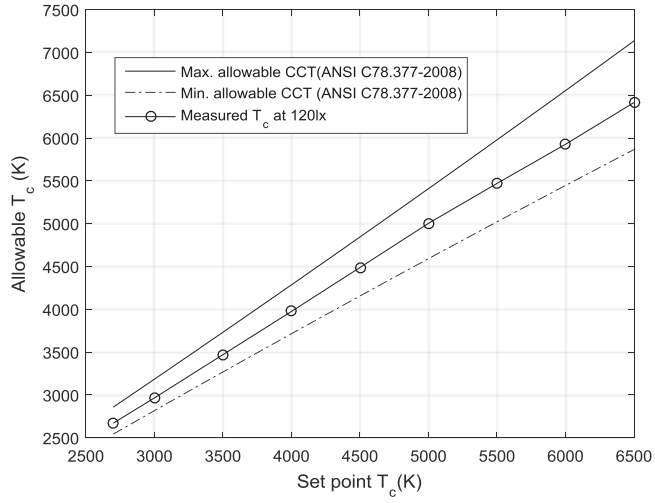

Fig. 21. Comparison of measured CCT with ANSI standard.

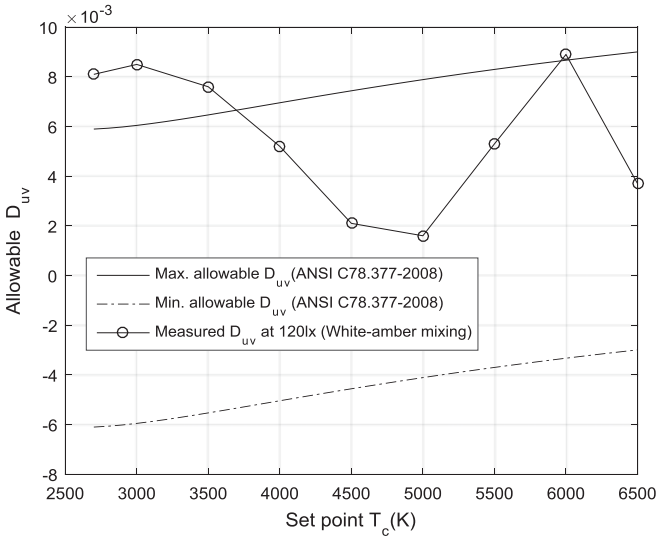

Fig. 22. Comparison of D_{uv} with ANSI standard for white-amber blending.

the constituents and their corresponding values of E_M, its position of the blending line is nearly fixed, barring the temperature dependence of the luminous parameters. The positioning of the R + G + R string to meet the requirements of symmetry with respect to the white LEDs has to be compromised. Additionally, these LEDs must be placed close enough so that the temperature difference between their cases is very small, failing which the values of the 18 constants of the model for luminous parameters become imprecise. Although the initial results in terms of D_{uv} and CRI improvement in the CCT range of 2500–4000 K range are encouraging, more trials with green LEDs with different values of the ratio $E_M(0)/I_{\mathrm{LED\_pk}}$ are required. Selection of white

LED is also an important factor: high-CRI white LEDs should be chosen in the blending process to get high CRI throughout the CCT range. The chromaticity of the white LED also should be as close as possible to the Planckian locus to improve the D_{uv}.

V. Conclusion

Based on a simple mathematical foundation, the design and operation of an LED lamp with wide-range CCT and illuminance control capability using two-component color blending have been described in this paper. The implementation uses only readily available components including a low-cost microcontroller. The average forward voltages of active LEDs are measured at runtime and the luminous parameters of the LEDs are estimated by using a simple algorithm. The method of estimation of parameters, which does not need any temperature measurement, demonstrates the capability of operation of the system over a wide ambient temperature range. A simple noniterative program for the controller has been presented. Experimental results demonstrate that the proposed approach for luminous parameter estimation yields more accurate results than those produced under the assumption of fixed luminous parameters. The proposed RBW LED lighting system has been compared with the ANSI standard for solid-state lighting products. Considering the wide range of available CCT, the error in CCT, D_{uv} and measured CRI of the blended light are acceptable for a large class of applications. An extension of the method has also been suggested, in which the values of the D_{uv} and CRI for the CCT range of 2500–6500 K can be greatly improved by replacement of the red LED string by a composite LED.

Acknowledgment

The first author wants to acknowledge Visvesvaraya Ph.D. scheme from Govt. of India and TEQIP-II for awarding the fellowship under the schemes and infrastructural facility in Illumination Engineering Laboratory, Department of Electrical Engineering, Jadavpur University, to carry out this research work.

References

[1] M. Cole, H. Clayton, and K. Martin, "Solid state lighting: The new normal in lighting," *IEEE Trans. Ind. Appl.*, vol. 51, no. 1, pp. 109–119, Jan./Feb. 2015.

[2] J. K. Kim and E. F. Schubert, "Transcending the replacement paradigm of a solid-state lighting," *Opt. Soc. Amer.*, vol. 16, no. 26, pp. 21835–21842, Dec. 2008.

[3] S. Golder, S. Mazumdar, and K. Ray, "A high efficiency DC to DC boost converter for white LED based lighting systems—An energy efficient, cost-effective approach for rural application," *Light Eng.*, vol. 15, no. 2, pp. 53–58, Nov. 2007.

[4] J. M. Gilman, M. E. Miller, and M. R. Grimaila, "A simplified control system for a daylight-matched LED lamp," *Lighting Res. Technol.*, vol. 45, no. 5, pp. 614–629, Oct. 2013.

[5] K.-C. Lin and C.-S. Lin, "The study of a novel control method of the mood lighting emulator," *Opt. Commun.*, vol. 350, pp. 71–76, Apr. 2015.

[6] G. Curcio, L. Piccardi, F. Ferlazzo, A. Maria, G. C. Burattini, and F. Bisegna, "LED lighting effect on sleep, sleepiness, mood and vigor," in *Proc. 16th Int. Conf. Environ. Elect. Eng.*, Jun. 7–10, 2016, pp. 1540–1545.

[7] P. R. Mills, S. C. Tomkins, and L. J. M. Schlangen, "The effect of high correlated colour temperature office lighting on employee wellbeing and work performance," *J. Circadian Rhythms*, vol. 2, no. 5, pp. 1–9, Jan. 2007.

[8] H. Jin, S. Jin, L. Chen, S. Cen, and K. Yuan, "Research on the lighting performance of LED street lights with different color temperatures," *IEEE Photon. J.*, vol. 7, no. 6, pp. 81–88, Dec. 2015.

[9] E. F. Schubert, *Light-Emitting Diodes*, 2nd ed. New York, NY, USA: Cambridge Univ. Press, 2006, pp. 332–346.

[10] S. Muthu, F. J. Schuurmans, and M. D. Pashley, "Red, green, and blue LEDs for white light illumination," *IEEE Trans. J. Sel. Topics Quantum Electron.*, vol. 8, no. 2, pp. 333–338, Mar./Apr. 2002.

[11] F.-C. Wang, C.-W. Tang, and B.-J. Huang, "Multivariable robust control for a red-green-blue LED lighting system," *IEEE Trans. Power Electron.*, vol. 25, no. 2, pp. 417–428, Feb. 2010.

[12] C.-W. Tang, B.-J. Huang, and S.-P. Ying, "Illumination and color control in red-green-blue light-emitting diode," *IEEE Trans. Power Electron.*, vol. 29, no. 9, pp. 4921–4937, Sep. 2014.

[13] H. Zhao and S. W. R. Lee, "Determination of driving current of RGB LEDs for white light illumination," in *Proc. 13th Int. Conf. Electron. Packag. Technol. High Density Packag.*, Aug. 13–16, 2012, pp. 1540–1545.

[14] M. Dyble, N. Narendran, A. Bierman, and T. Klein, "Impact of dimming white LEDs: Chromaticity shifts due to different dimming methods," *Proc. SPIE*, vol. 5941, pp. 291–299, 2005.

[15] S. K. Ng, K. H. Loo, Y. M. Lai, and C. K. Tse, "Color control system for RGB LED with application to light sources suffering from prolonged aging," *IEEE Trans. Ind. Electron.*, vol. 61, no. 4, pp. 1788–1798, Apr. 2014.

[16] X. H. Qu, S. C. Wong, and C. K. Tse, "Temperature measurement technique for stabilizing the light output of RGB LED lamps," *IEEE Trans. Instrum. Meas.*, vol. 59, no. 3, pp. 661–670, Jul. 2010.

[17] K. H. Loo, Y. M. Lai, S. C. Tan, and C. K. Tse, "On the color stability of phosphor-converted white LEDs under DC, PWM, and bilevel drive," *IEEE Trans. Power Electron.*, vol. 27, no. 2, pp. 974–984, Feb. 2012.

[18] S. K. Ng, K. H. Loo, Y. M. Lai, and C. K. Tse, "Color control system for RGB LED with application to light sources suffering from prolonged aging," *IEEE Trans. Ind. Electron.*, vol. 61, no. 4, pp. 1788–1798, Apr. 2014.

[19] C. H. Miao, "Color temperature adjustable lamp," U.S. Patent US8159125B2, Apr. 2012.

[20] K. Jonsson, "Light with changeable color temperature," U.S. Patent US20120146505A1, Jun. 2012.

[21] A. T. L. Lee, H. Chen, S.-C. Tan, and S. Y. Hui, "Precise dimming and color control of LED systems based on color mixing," *IEEE Trans. Power Electron.*, vol. 31, no. 1, pp. 65–80, Jan. 2016.

[22] H.-T. Chen, S. Tan, and S. Y. Hui, "Nonlinear dimming and correlated color temperature control of bicolor white LED systems," *IEEE Trans. Power Electron.*, vol. 30, no. 12, pp. 6934–6947, Dec. 2015.

[23] *Color Tuning with Lutron Controls*, Lutron, Coopersburg, PA, USA, Application Note, 2016. [Online]. Available: http://www.lutron.com/TechnicalDocumentLibrary/048579.pdf

[24] *Tunable White Light Engines for Warm Dimming and CCT Tuning, LED Engin, LuxiTune*, San Jose, CA, USA, User's Manual, 2017. [Online]. Available: http://www.ledengin.com/files/products/luxitune/LTC-Q3T1xxxxH-1Bx.pdf

[25] S. Muthu and J. Gaines, "Red, green, and blue LED-based white light source: Implementation challenges and control design," in *Proc. Ind. Appl. Conf.*, 2003, pp. 515–522.

[26] H. Chen, D. Y. Lin, S. C. Tan, and S. Y. Hui, "Chromatic, photometric and thermal modeling of LED systems with nonidentical LED devices," *IEEE Trans. Power Electron.*, vol. 29, no. 12, pp. 6636–6647, Dec. 2014.

[27] P. Deurenberg, C. Hoelen, J. van Meurs, and J. Ansems, "Achieving color point stability in RGB multi-chip LED modules using various color control loops," *Proc. SPIE*, vol. 5941, pp. 63–74, 2005.

[28] S. Muthu, F. J. Schuurmans, and M. D. Pashley, "Red, green, and blue LED based white light generation: Issues and control," in *Proc. Ind. Appl. Conf.*, Oct. 2002, pp. 327–333.

[29] M. M. Sisto and J. Gauvin, "Accurate chromatic control and color rendering optimization in LED lighting systems using junction temperature feedback," *Proc. SPIE*, vol. 9190, Sep. 2014, Art. no. 919002.

[30] J. M. Yurtseven, S. Mete, and S. Onayagil, "The effect of temperature and driving current on the key parameters of commercially available, high-power, white LEDs," *Lighting Res. Technol.*, vol. 48, no. 5, pp. 943–965, Feb. 2015.

[31] S. Chhajed, Y. Xi, Y. L. Li, T. Gessmann, and E. F. Schubert, "Influence of junction temperature on chromaticity and color-rendering properties of trichromatic white-light sources based on light-emitting diodes," *J. Appl. Phys.*, vol. 97, no. 5, pp. 054506-1–054506-8, Mar. 2005.
[32] A. Keppens, W. R. Ryckaert, G. Deconinck, and P. Hanselaer, "Modeling high power light-emitting diode spectra and their variation with junction temperature," *J. Appl. Phys.*, vol. 108, no. 4, pp. 043104-1–043104-7, Aug. 2010.
[33] L. De Oto and T. E. Clary, "LED brightness compensation system and methods," Eur. Patent 190 158 7A2, Mar. 19, 2008.
[34] J. B. Murdoch, *Illumination Engineering—From Edison's Lamp to Laser*, 1st ed. New York, NY, USA: Macmillan, 1985, p. 541.
[35] D. Malacara, *Color Vision and Colorimetry: Theory and Applications*. Bellingham, WA, USA: SPIE Press, 2002.
[36] N. Pousset, B. Rougie´, and A. Razet, "Impact of current supply on LED colour," *Lighting Res. Technol.*, vol. 42, no. 4, pp. 371–383, Aug. 2010.
[37] C. S. McCamy, "Correlated color temperature as an explicit function of chromaticity coordinates," *Color Res. Appl.*, vol. 17, no. 2, pp. 142–144, Apr. 1992.
[38] *8-Bit AVR Microcontroller ATmega32A Datasheet Complete*, ATmega32A, Atmel Corp., San Jose, CA, USA, 2016. [Online]. Available: http://www.atmel.com/images/atmel-8155-8-bit microcontroller-avr-atmega32a_datasheet.pdf
[39] J. D. Bullough, K. S. Hickcox, T. R. Klein, and N. Narendran, "Effects of flicker characteristics from solid-state lighting on detection, acceptability and comfort," *Lighting Res. Technol.*, vol. 43, no. 3, pp. 337–348, Jul. 2011.
[40] C.-C. Wu, N.-C. Hu, J.-N. Chen, and H.-I. Chang, "Parameterised LED current regulator for pulse width modulation switch delay for accurate color mixing in multi-LED light sources," *Lighting Res. Technol*., vol. 43, no. 2, pp. 171–186, Dec. 2012.
[41] *IEEE Recommended Practices for Modulating Current in High-Brightness LEDs for Mitigating Health Risks to Viewers*, IEEE Standard 1789-2015, Jun. 2015.
[42] B. T. Irving and M. M. Jovanovic, "Analysis and design of self-oscillating flyback converter," in *Proc. 17th Annu. IEEE Appl. Power Electron. Conf.*, vol. 2, Mar. 2002, pp. 897–903.
[43] D. G. Lamar, M. Arias, A. Rodriguez, A. Fernandez, M. M. Hernando, and J. Sebastian, "Design-oriented analysis and performance evaluation of a low-cost high-brightness LED driver based on flyback power factor corrector," *IEEE Trans. Ind. Electron.*, vol. 60, no. 7, pp. 2614–2626, Jul. 2013.
[44] Y. Ohno, "Color quality of lighting and metrics," *EPA Energy Star Lighting Webinar, Evaluating Color Quality*, Mar. 31, 2016. [Online]. Available: https://www.energystar.gov/sites/default/files/asset/document/Energy%20Star%20webinar%20Presentation%20-%20Ohno%202.pdf
[45] *Specifications for Chromaticity of Solid State Lighting Products, Amer. Nat. Standard*, ANSI C78.377, 2008.

Rajib Malik received the B.E. degree in applied electronics and instrumentation engineering from Burdwan University, Bardhaman, India, in 2010, and the M.E. degree in illumination engineering under electrical engineering from Jadavpur University, Kolkata, India, in 2013, where he is currently working toward the Ph.D. degree in electrical engineering.

His research interests include solar-based smart lighting systems, electronic converters for lighting applications, embedded control and color control of LED lighting.

Kalyan Kumar Ray received the B.E.E. degree from Jadavpur University, Kolkata, India, in 1968, where he was adjudged the best student in the Faculty of Engineering and Technology, the M.Tech. degree from the Indian Institute of Technology, Kanpur, India, in 1970, and the Ph.D. degree from Jadavpur University in 1979, all in electrical engineering.

He was a Senior Research Assistant with the Indian Institute of Technology, Kanpur, from 1968 to 1973. In 1973, he joined Jadavpur University, Kolkata, India, as a Lecturer. He served in the Departments of Electrical Engineering and Instrumentation and Electronics Engineering for 39 years and retired as a Professor. He was Principal Investigator in several Government-funded projects. He is currently a Consultant to industries manufacturing electronic systems. His primary research interests include control of power electronic converters, embedded control and instrumentation, solar photovoltaic conversion, and vehicular electronics.

Saswati Mazumdar received the B.E.E., M.E., and Ph.D. degrees in electrical engineering (EE) from Jadavpur University (JU), Kolkata, India, in 1982, 1984, and 1996, respectively.

She worked first as CSIR Senior Research Fellow, then System Development Engineer in a DOE-funded Project in the Department of EE, JU. From 1987, she joined in teaching in the department of EE, JU. She acted as Director of School of Illumination Science, Engineering and Design, JU from 2006 to 2014. She is currently working as a Professor in the Department of EE, JU, Kolkata, India. She has now 30 years of experience in lighting research and teaching. She developed a modernized Illumination Engineering Laboratory in Department of EE, JU. She has founded one full-time Master's Course on illumination engineering and another part-time Master's course on illumination technology and design in JU. She has executed a large number of R&D and Consultancy Projects on illumination and allied fields. Her primary research areas are controllers of lighting systems, renewable energy-based lighting systems, smart lighting systems, LEDs and LASER communication, interior and exterior lighting design, and color control of modern lighting systems.